

Development of Hydrogen-Rich Benzoxazine Resins with Low Polymerization Temperature for Space Radiation Shielding

Daniela Iguchi,[†] Seishi Ohashi,[†] Ghizelle J. E. Abarro,^{†,‡} Xianze Yin,^{†,||} Scott Winroth,^{§,b} Chris Scott,[§] Molly Gleydura,^{†,⊥} Lin Jin,[†] Nithya Kanagasagar,[†] Cherie Lo,[†] Carlos Rodriguez Arza,[†] Pablo Froimowicz,^{†,#} and Hatsuo Ishida^{*,†,ib}

[†]Department of Macromolecular Science and Engineering, Case Western Reserve University, 10900 Euclid Avenue, Cleveland, Ohio 44106-7202, United States

[‡]University of the Philippines Diliman, Diliman, Quezon City 1101, The Philippines

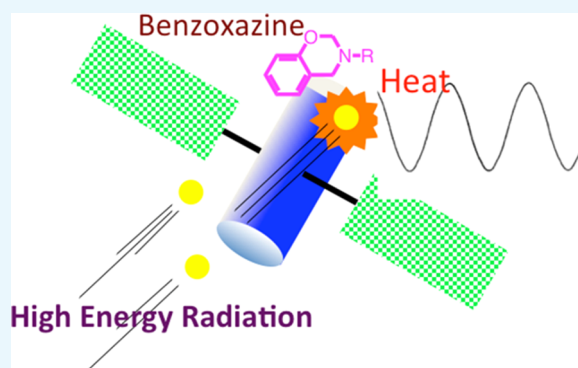
[§]Material Answers LLC, 66 Bucksin Drive, Weston, Massachusetts 02493, United States

^{||}School of Materials Science and Engineering, Wuhan Textile University, Wuhan 430200, China

[⊥]Hathaway Brown School, Shaker Heights, Ohio 44122, United States

[#]Design and Chemistry of Macromolecules Group, Institute of Technology in Polymers and Nanotechnology (ITPN), UBA-CONICET, FIUBA, FADU, University of Buenos Aires, Pabellón III, subsuelo, Ciudad Universitaria, 1428 Buenos Aires, Argentina

ABSTRACT: A systematic study has been carried out to develop a material with significant protection properties from galactic cosmic radiation and solar energetic particles. The research focused on the development of hydrogen-rich benzoxazines, which are particularly effective for shielding against such radiation. Newly developed benzoxazine resin can be polymerized at 120 °C, which meets the low-temperature processing requirements for use with ultrahigh molecular weight polyethylene (UHMWPE) fiber, a hydrogen-rich composite reinforcement. This highly reactive benzoxazine resin also exhibits low viscosity and good shelf-life. The structure of the benzoxazine monomer is confirmed by proton nuclear magnetic resonance and Fourier transform infrared spectroscopy. Polymerization behavior and thermal properties are evaluated by differential scanning calorimetry and thermogravimetric analysis. Dynamic mechanical analysis is used to study chemorheological properties of the benzoxazine monomer, rheological properties of the cross-linked polybenzoxazine, and rheological properties of UHMWPE-reinforced polybenzoxazine composites. The theoretical radiation shielding capability of the composite is also evaluated using computer-based simulations.



1. INTRODUCTION

In recent years, benzoxazines have generated great interest given their capacity to polymerize and generate polybenzoxazines (PBZs). Polybenzoxazines are thermosets with unique and exciting attributes, such as low flammability,¹ near-zero shrinkage,² high thermal stability,³ and excellent mechanical properties.^{3d,4} However, one of the most important features of benzoxazines is their versatile molecular design capability,⁵ which makes it possible to tailor the properties at the molecular level to obtain targeted characteristics that are particularly advantageous for specific applications.

The development of new materials to effectively protect astronauts from harmful radiation has been an important issue since the beginning of space travel. The wide variety of radiation encountered in space includes galactic cosmic radiation (GCR) and solar energetic particles (SEPs). Aluminum is widely used for spacecraft construction, especially structural components. However, aluminum does not shield

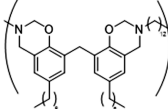
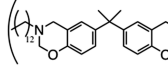
effectively against GCR and SEP. This necessitates the addition of other shielding materials into the spacecraft design, resulting in a heavier and larger craft. A variety of other materials have been studied, including hydrogenated graphite nanofibers, lithium hydride, polysulfone, polyetherimide, liquid methane, carbon fiber composites, epoxy, and polyethylene (PE).⁶ Recent studies have incorporated nanosized particles made of metal, metal oxides, and coated polymers into high-strength polymer matrices.^{6b,7} Much of the attention on radiation shielding has shifted to polymer composites because of the potential for high protection efficiency and high specific properties, such as specific strength and specific modulus.⁸ Hydrogen-rich materials are known to be effective for shielding against GCR and SEP; thus, composites with a hydrogen-rich

Received: July 9, 2018

Accepted: September 7, 2018

Published: September 21, 2018

Table 1. Initial Benzoxazine Compounds Studied

Compound	No. of H atoms per repeating unit	Average density (g/cm ³)	MW of repeat unit (g/mol)	H concentration ($\frac{\text{H atoms}}{\text{cm}^3} \times 10^{23}$)
Poly(BNP-daC ₁₂) 	76	1.03	701.098	0.673
Poly(BPA-daC ₁₂) 	44	1.12	476.68	0.625

matrix and ultrahigh molecular weight polyethylene (UHMWPE) fiber reinforcement can provide both shielding and structural utility. A recent patent by Kaul et al. describes a three-layered composite that can be used for space vehicles or space habitat structures. The outer layer is an epoxy composite reinforced with UHMWPE and graphite fibers. This layer is intended to provide protection against micrometeoroid impacts. The sandwiched layer, an UHMWPE fiber-reinforced PE composite, is primarily constructed for radiation protection. As an integral structural member, the innermost layer is made of ceramic tiles.⁹ Polyethylene (CH₂)_n is a relatively inexpensive polymer that possesses a high concentration of hydrogen atoms within its molecular structure.¹⁰ In-flight studies were also undertaken to confirm its efficiency.¹¹ PE slabs have been used to improve shielding in some quarters of the Intcon (ISS).¹² However, PE slabs provide little or no structural utility.

The most significant challenge encountered during this project was related to resin development. The newly developed resins reported in this publication were required to possess the following characteristics: (i) the resin must have high hydrogen concentration approaching that of polyethylene; (ii) the resin can polymerize and cross-link at 120 °C via oxazine ring-opening reaction in a reasonable processing time; and (iii) the resin must have adequate shelf-life for commercial viability. The seemingly contradictory requirements of (ii) and (iii) are important from the manufacturing point of view, whereas the requirement (i) is needed for the material to successfully protect astronauts from GCR and SEP.

The current paper is the result of more than a decade of developmental efforts. In the early stages of development, we successfully developed high hydrogen-containing benzoxazine resins that can be polymerized at 120 °C. Compounds shown in Table 1 satisfied the hydrogen concentration requirement. However, these resins polymerized only through the condensation reaction of the terminal groups of the polybenzoxazine main chain. Thus, this led to mostly oligomeric, linear polybenzoxazines that did not fulfill the requirement of polymerization via oxazine ring opening.

Further attempts to develop a long-chain alkyl group bearing ortho-functional bisphenol as a raw material allowed an increase in the hydrogen concentration and a reduction in the polymerization temperature. Recently, reactivity and properties of isomeric benzoxazines have been reported¹³ where bisphenols based on the substituent ortho to the phenolic group have unexpectedly shown superior properties

to those of the para position. Use of the ortho position also improved reactivity while maintaining a high concentration of hydrogen. However, both reactivity and shelf-life were inadequate, and the processability requirement was not met.

It has been a long and sustaining effort in the benzoxazine chemistry community to understand the mechanism of increased rate of polymerization and develop compounds that polymerize at low temperature with good shelf-life. Understanding the polymerization mechanism of benzoxazines is an elusive target despite significant efforts by many researchers.¹⁴

Adding a rigid moiety in the backbone seems to accelerate the rate of polymerization. This phenomenon was reported for a liquid crystal forming monomer¹⁵ as well as a diacetylene-bearing molecule.¹⁶ Near neighbor effect is also reported to be effective in reducing the polymerization temperature.^{3a,17} Another approach is to form intramolecular five- or six-membered hydrogen bonding to the oxazine ring, which significantly influences the ring-opening equilibrium.¹⁸ Naturally, adding initiators and/or catalyst will help reduce the temperature as well.^{14e,19} One popular approach is to understand the role of the substituent, either on the phenolic or amine moiety, in influencing the oxazine ring-opening equilibrium. Influence of the substituents on the oxazine reactivity has been a popular subject.^{17c,d,20} Yet, to date, no benzoxazine monomers have been reported that possess the characteristics of a low polymerization temperature of 120 °C and a sufficient shelf-life.

It was, therefore, the purpose of this work to develop an approach to synthesize benzoxazine resins that can be polymerized at 120 °C, provide a shelf-life of several months (when stored under refrigerated conditions), and possess a high hydrogen concentration that is sufficient to protect astronauts from GCR and SEP. In this study, a series of bifunctional benzoxazines were synthesized from meta-substituted alkoxy phenols, particularly methoxy and butoxyphenol, and diamines with different hydrocarbon chain lengths. The structures of the synthesized monomers were analyzed by proton nuclear magnetic resonance (¹H NMR) and Fourier transform infrared (FT-IR) spectroscopy. The trend in polymerization temperature and thermal stability was studied by differential scanning calorimetry (DSC) and thermogravimetric analysis (TGA). Due to small structural variations in the isomers, it was not possible to separate and purify the isomers independently.

2. EXPERIMENTAL SECTION

2.1. Materials. 3-Butoxyphenol (97%), 3-methoxyphenol (98%), and 1,12-diaminododecane (98%) were purchased from Tokyo Chemical Industry Co. Paraformaldehyde (96% extra pure), 1,2-diaminoethane (>98%), 1,4-diaminobutane (>98%), 1,6-diaminohexane (>99%), and 1,8-diaminooctane (98%) were purchased from Sigma-Aldrich Co. Formalin (37% by weight formaldehyde solution), hydrochloric acid, sodium bicarbonate, magnesium sulfate anhydrous, chloroform, and ethyl ether were purchased from Fisher Scientific Inc. and used as received. Plain-woven Spectra 1000 UHMWPE fabric (Style 932) was purchased from SAATI Americas Corp.

2.2. Synthesis of 3MOP-daC2 and 3MOP-daC4. 3-Methoxyphenol, the corresponding diamine (1,2-diaminoethane or 1,4-diaminobutane), and formalin were mixed in stoichiometric amounts (mole ratio, 2:1:4.2) in a single-neck reaction flask. A slight excess of formalin was used. Chloroform (5 mL/g of reactants) was added to the flask. The reaction mixture was refluxed with stirring at room temperature for 4 h. The crude reaction products were washed three times with 1 N NaOH solution and rinsed three times with distilled water. The products were dried over magnesium sulfate anhydrous overnight and filtered to remove the salt. The products were then precipitated by rinsing with hexane. The purified benzoxazine monomer was dried under vacuum for over 48 h to obtain the isomer mixtures as a pale yellow wax. The resulting benzoxazine monomers are abbreviated as 3MOP-daC2 for 1,2-diaminoethane and 3MOP-daC4 for 1,4-diaminobutane. It is understood that each abbreviation includes the three isomers (5,5'-, 5,7'-, and 7,7'-). The chemical structure of these isomers is discussed in a later section. The yields for 3MOP-daC2 and 3MOP-daC4 were 67 and 65%, respectively.

2.2.1. 3MOP(7)-daC₂. ¹H NMR (CDCl₃, 600 MHz ¹H, 298 K, δ): 2.95 (s, 4H, N-(CH₂)₂-N), 3.75 (s, 6H, O-CH₃), 3.97 (s, 4H, N-CH₂-Ar), 4.87 (s, 4H, O-CH₂-N), 6.34 (d, J = 2.4 Hz, 2H, H-8), 6.45 (dd, J = 2.4 and 8.4 Hz, 2H, H-6), 6.83 (d, J = 8.4 Hz, 2H, H-5).

2.2.2. 3MOP(5)-daC₂. ¹H NMR (CDCl₃, 600 MHz ¹H, 298 K, δ): 2.95 (s, 4H, N-(CH₂)₂-N), 3.75 (s, 6H, O-CH₃), 3.95 (s, 4H, N-CH₂-Ar), 4.85 (s, 4H, O-CH₂-N), 6.41 (dd, J = 1.2 and 7.8 Hz, 4H, H-6), 6.43 (dd, J = 1.2 and 7.8 Hz, 4H, H-8), 7.06 (dd, J = 7.8 Hz, 2H, H-7).

2.2.3. 3MOP(7)-daC₄. ¹H NMR (CDCl₃, 600 MHz ¹H, 298 K, δ): 1.60 (ws, 4H, N-CH₂-(CH₂)₂-CH₂-N), 2.75 (ws, 4H, N-CH₂-(CH₂)₂-CH₂-N), 3.75 (s, 6H, O-CH₃), 3.92 (s, 4H, N-CH₂-Ar), 4.83 (4H, O-CH₂-N), 6.34 (d, J = 2.4 Hz, 2H, H-8), 6.45 (dd, J = 2.4 and 7.8 Hz, 2H, H-6), 6.84 (d, J = 7.8 Hz, 2H, H-5).

2.2.4. 3MOP(5)-daC₄. ¹H NMR (CDCl₃, 600 MHz ¹H, 298 K, δ): 1.60 (ws, 4H, N-CH₂-(CH₂)₂-CH₂-N), 2.75 (ws, 4H, N-CH₂-(CH₂)₂-CH₂-N), 3.79 (s, 6H, O-CH₃), 3.91 (s, 4H, N-CH₂-Ar), 4.80 (4H, O-CH₂-N), 6.42 (4H, H-6 and H-8), 7.06 (dd, J = 8.4 Hz, 2H, H-7).

2.3. Synthesis of 3MOP-daC6, 3MOP-daC8, and 3MOP-daC12. 3-Methoxyphenol, the corresponding diamine (1,6-diaminohexane, 1,8-diaminooctane, or 1,12-diaminododecane), and paraformaldehyde were mixed in stoichiometric amounts (mole ratio, 2:1:4.2) in a round-bottom flask. A slight excess of paraformaldehyde was used. Chloroform (5 mL/g of reactants) was added to the round-bottom flask. The solution was stirred at 60 °C for 7 h. The completed reaction product

was washed three times with 1 N NaOH and three times with distilled water. The product was dried over magnesium sulfate anhydrous overnight. The solution was filtered to remove the salt. After evaporating the solvent, the isomer mixture was dried in a vacuum oven to obtain a pale yellow wax in all cases. The resulting benzoxazine monomers are abbreviated as 3MOP-daC6 for 1,6-diaminohexane, 3MOP-daC8 for 1,8-diaminooctane, and 3MOP-daC12 for 1,12-diaminododecane. Again, each abbreviation includes the three isomers for each diamine. The reaction yield was 69% for 3MOP-daC6 and 3MOP-daC8, and 71% for 3MOP-daC12.

2.3.1. 3MOP(7)-daC₆. ¹H NMR (CDCl₃, 600 MHz ¹H, 298 K, δ): 1.35 (ws, 4H, N-CH₂-CH₂-(CH₂)₂-CH₂-CH₂-N), 1.55 (ws, 4H, N-CH₂-CH₂-(CH₂)₂-CH₂-CH₂-N), 2.71 (ws, 4H, N-CH₂-CH₂-(CH₂)₂-CH₂-CH₂-N), 3.75 (s, 6H, O-CH₃), 3.92 (s, 4H, N-CH₂-Ar), 4.83 (s, 2H, O-CH₂-N), 6.34 (d, J = 2.4 Hz, 2H, H-8), 6.45 (dd, J = 2.4 and 8.4 Hz, 2H, H-6), 6.84 (d, J = 8.4 Hz, 2H, H-5).

2.3.2. 3MOP(5)-daC₆. ¹H NMR (CDCl₃, 600 MHz ¹H, 298 K, δ): 1.35 (ws, 4H, N-CH₂-CH₂-(CH₂)₂-CH₂-CH₂-N), 1.55 (ws, 4H, N-CH₂-CH₂-(CH₂)₂-CH₂-CH₂-N), 2.71 (ws, 4H, N-CH₂-CH₂-(CH₂)₂-CH₂-CH₂-N), 3.79 (s, 6H, O-CH₃), 3.90 (s, 4H, N-CH₂-Ar), 4.80 (s, 2H, O-CH₂-N), 6.42 (dd, J = 8.4 Hz, 4H, H-6 and H-8), 7.06 (dd, J = 8.4 Hz, 2H, H-7).

2.3.3. 3MOP(7)-daC₈. ¹H NMR (CDCl₃, 600 MHz ¹H, 298 K, δ): 1.30 (ws, 8H, N-CH₂-CH₂-(CH₂)₄-CH₂-CH₂-N), 1.55 (ws, 4H, N-CH₂-CH₂-(CH₂)₂-CH₂-CH₂-N), 2.71 (ws, 4H, N-CH₂-CH₂-(CH₂)₂-CH₂-CH₂-N), 3.75 (s, 6H, O-CH₃), 3.92 (s, 4H, N-CH₂-Ar), 4.83 (s, 2H, O-CH₂-N), 6.34 (d, J = 2.4 Hz, 2H, H-8), 6.45 (dd, J = 2.4 and 8.4 Hz, 2H, H-6), 6.84 (d, J = 8.4 Hz, 2H, H-5).

2.3.4. 3MOP(5)-daC₈. ¹H NMR (CDCl₃, 600 MHz ¹H, 298 K, δ): 1.30 (ws, 8H, N-CH₂-CH₂-(CH₂)₄-CH₂-CH₂-N), 1.55 (ws, 4H, N-CH₂-CH₂-(CH₂)₂-CH₂-CH₂-N), 2.71 (ws, 4H, N-CH₂-CH₂-(CH₂)₂-CH₂-CH₂-N), 3.79 (s, 6H, O-CH₃), 3.90 (s, 4H, N-CH₂-Ar), 4.80 (s, 2H, O-CH₂-N), 6.42 (dd, J = 8.4 Hz, 4H, H-6 and H-8), 7.06 (dd, J = 8.4 Hz, 2H, H-7).

2.4. Synthesis of 3BOP-daC12. 3-Butoxyphenol, 1,12-diaminododecane, and paraformaldehyde were mixed in stoichiometric amounts (mole ratio, 2:1:4.2) in a round-bottom flask. A slight excess paraformaldehyde was used. Chloroform (5 mL/g of reactants) was added to the round-bottom flask. The solution was stirred at 60 °C for 7 h. The completed reaction product was washed three times with 1 N NaOH and three times with distilled water. The product was dried over magnesium sulfate anhydrous overnight. The solution was filtered to remove the salt. After evaporating the solvent, the isomer mixture was dried in a vacuum oven to obtain a pale yellow wax in all cases. The reaction yield for the resulting benzoxazine monomer, abbreviated as 3BOP-daC12, was 75%.

2.4.1. 3BOP(7)-daC₁₂. ¹H NMR (CDCl₃, 600 MHz ¹H, 298 K, δ): 0.96 (t, 6H, OCH₂CH₂CH₂CH₃), 1.26 (ws, 16H, N-CH₂-CH₂-(CH₂)₈-CH₂-CH₂-N), 1.28 (ws, 4H, N-CH₂-CH₂-(CH₂)₈-CH₂-CH₂-N), 1.47 (m, 4H, OCH₂CH₂CH₂CH₃), 1.74 (m, 4H, OCH₂CH₂CH₂CH₃), 2.71 (ws, 4H, N-CH₂-CH₂-(CH₂)₂-CH₂-CH₂-N), 3.90 (s, 4H, OCH₂CH₂CH₂CH₃), 3.92 (s, 4H, N-CH₂-Ar), 4.83 (s, 2H, O-CH₂-N), 6.33 (ws, 2H, H-8), 6.45 (d, J = 8.5 Hz, 2H, H-6), 6.82 (d, J = 8.5 Hz, 2H, H-5).

2.4.2. *3BOP(5)-daC₁₂*. ¹H NMR (CDCl₃, 600 MHz ¹H, 298 K, δ): 0.96 (t, 6H, OCH₂CH₂CH₂CH₃), 1.26 (ws, 16H, N-CH₂-CH₂-(CH₂)₈-CH₂-CH₂-N), 1.28 (ws, 4H, N-CH₂-CH₂-(CH₂)₈-CH₂-CH₂-N), 1.47 (m, 4H, OCH₂CH₂CH₂CH₃), 1.74 (m, 4H, OCH₂CH₂CH₂CH₃), 2.71 (ws, 4H, N-CH₂-CH₂-(CH₂)₂-CH₂-CH₂-N), 3.88 (s, 4H, OCH₂CH₂CH₂CH₃), 3.91 (s, 4H, N-CH₂-Ar), 4.81 (s, 2H, O-CH₂-N), 6.40 (dd, $J = 8$ Hz, 4H, H-6 and H-8), 7.03 (dd, $J = 8$ Hz, 2H, H-7).

2.5. Cross-Linking of Benzoxazines. All benzoxazine resins were cross-linked using a heating schedule that included a dwell at 120 °C for at least 2 h. Since the resins described in the current paper are intended for use as matrices in composites with UHMWPE fiber reinforcements (whose properties start degrading at 130 °C in several hours), polymerization conditions were selected so as to not degrade the properties of the reinforcing fibers.

2.6. Preparation of UHMWPE Fiber-Reinforced Polybenzoxazine Composites. Composite samples, containing UHMWPE fiber reinforcements and poly(3BOP-daC₁₂) matrices, were fabricated using a vacuum bagging process. A flat mold, constructed from a 30.5 × 30.5 × 0.953 cm³ (12 × 12 × 0.375 in.³)-polished aluminum plate, was used as the primary fabrication tool. An exploded assembly drawing of the mold is shown below in Figure 1. Composites were prepared

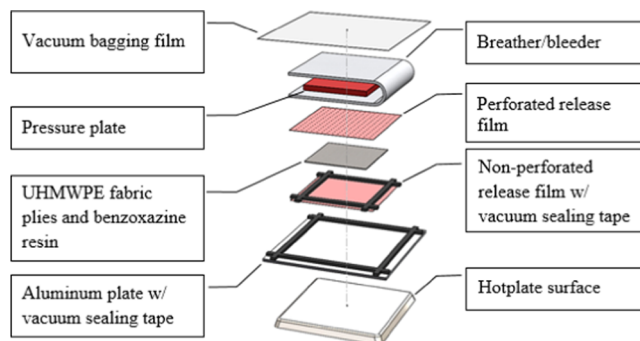


Figure 1. Exploded assembly drawing of the vacuum bagging mold.

by the hand lay-up method followed by vacuum bagging operation for polymerization and consolidation. Benzoxazine resin was spread onto UHMWPE fabric plies using a spatula and plastic squeegee. A large ceramic hotplate was placed under the aluminum mold and used as the heat source.

Consolidation and polymerization of all composites were achieved by simultaneously applying vacuum and heating the surface of the mold. The surface temperature of the aluminum mold was monitored and recorded throughout the polymerization cycle using surface-mounted thermocouples. A Welch ChemStar 1400N vacuum pump was used to apply vacuum to the mold. The pump was connected to the mold using vacuum tubing and a through-bag vacuum connector located on the top surface of the breather layer. A photograph of the equipment setup is provided below in Figure 2.

A plot of a typical composite polymerization cycle is provided below in Figure 3. An initial ramp and hold at 80 °C was performed to remove any excess moisture from the resin prior to polymerization. The resin was then polymerized at 120 °C for at least 2 h. The composite was under full vacuum (approx. 98 kPa or 29 in. Hg) during the entire polymerization cycle.

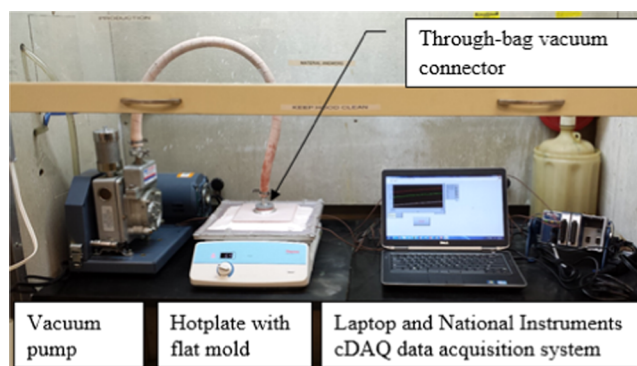


Figure 2. Photograph of composite fabrication equipment. (Photo is a courtesy of S. Winroth.)

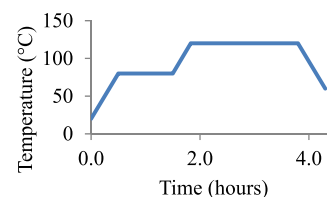


Figure 3. Plot of typical composite polymerization cycle.

After completion of the polymerization cycle, the entire aluminum mold was removed from the hotplate, placed on a cooling rack, and allowed to cool to room temperature. Vacuum continued to be applied during cooling to prevent warping of the composite plate. Thermocouple temperature was also monitored during cooling, and the composite was allowed to cool to approximately 60 °C prior to removal from the mold. Composite plates were visually inspected for defects after being removed from the mold. Excess resin flash and vacuum sealing tape were removed from the edges of the composite plates using a razor blade.

Composite samples were fabricated for mechanical testing. Two composite samples, each having nominal dimensions of 254 mm × 254 mm × 1.5 mm, were fabricated to generate specimens for tensile testing. Each composite was reinforced with eight plies of plain-woven Spectra 1000 fabric (Style 932), which had a nominal ply thickness of approximately 0.19 mm.

The appearance of the composite surfaces, including the as-molded surface and surfaces resulting from laser cutting and waterjet cutting, was similar to that of other composites manufactured commercially for structural applications. Composite samples were cross-sectioned using a waterjet cutter and then wet-polished with successively finer grades of silicon carbide sandpaper, down to 600 grit. The cross-sections were examined using stereomicroscopy. Examination revealed excellent infiltration of the resin into the reinforcing fibers and consolidation of the composites.

A fiber volume fraction (V_f) of approximately 60% was targeted for all composites. The volume fraction of fiber in each composite sample was calculated from empirical data as a quality control measure. This ensured that all composites contained the proper amounts of fiber and resin. The volume of fiber in each composite sample was determined by dividing the mass of UHMWPE fabric in the sample (weighed prior to lay-up) by the density of UHMWPE fabric (0.97 g/cm³). Total composite volume was calculated using dimensional measurements that were taken for each sample after processing was

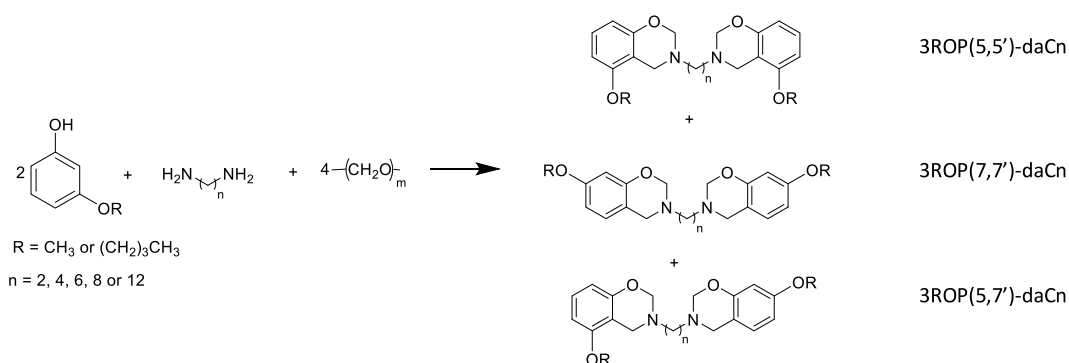


Figure 4. General synthesis scheme showing the mixture of three possible isomers.

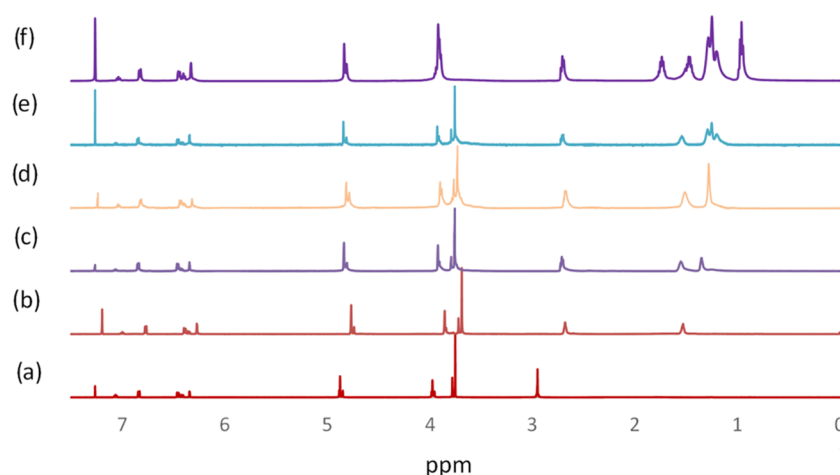


Figure 5. ^1H NMR spectra of (a) 3MOP-daC2, (b) 3MOP-daC4, (c) 3MOP-daC6, (d) 3MOP-daC8, (e) 3MOP-daC12 in CDCl_3 , (f) 3BOP-daC12 in CDCl_3 .

completed. Average fiber volume fraction was calculated as $59.2 \pm 3.0\%$ for tensile testing composites.

2.7. Equipment and Characterization. Molecular structures were studied using proton nuclear magnetic resonance (^1H NMR) spectra obtained on Varian Oxford AS600 with a proton frequency of 600 MHz. The solvent and internal standard used were deuterated chloroform (CDCl_3) and tetramethylsilane, respectively. For integrated intensity measurements, the relaxation time was set at 10 s with an average of 16 transients.

For further structural analysis, Fourier transform infrared (FT-IR) spectroscopic analysis was also performed using a Bomem Michelson MB 110 spectrophotometer with deuterated triglycine sulfate detector. A small amount of sample was sandwiched between two KBr plates. For each sample, 32 scans were accumulated and averaged at a resolution of 4 cm^{-1} to obtain the final FT-IR absorption spectrum.

Thermally induced transitional behavior of the benzoxazines was studied using differential scanning calorimetry (DSC) on a TA Instruments Modulated DSC model 2920 at a heating ramp rate of $10 \text{ }^\circ\text{C}/\text{min}$ with a nitrogen gas purge rate of 60 mL/min. Approximately 1 mg of sample was pressed in a hermetic aluminum pan with lid. Thermal stability of the cross-linked benzoxazines was studied using thermogravimetric analysis (TGA) on a TA Instruments model High-Res TGA 2950 at a heating ramp rate of $10 \text{ }^\circ\text{C}/\text{min}$ with a nitrogen gas purge rate of 60 mL/min.

Dynamic mechanical analysis (DMA) was used to determine rheological data using a Rheometrics RMS-800 in a torsional

mode with the sample size of the composite being $6 \text{ mm} \times 60 \text{ mm} \times 1 \text{ mm}$. The frequency of the torsional motion was 1 Hz with a temperature ramp rate of $2 \text{ }^\circ\text{C}/\text{min}$. A strain sweep was first performed to determine the largest possible strain to judge the linear viscoelastic limit and optimize the sensitivity and reproducibility.

3. RESULTS AND DISCUSSION

3.1. Structural and Property Characterization of Benzoxazine Monomers. The synthesis of the benzoxazines was done following the scheme shown in Figure 4 where the numbers in the parenthesis indicates the position of the alkoxy group with respect to the oxygen atom.

3.1.1. ^1H NMR Analysis. NMR spectroscopy was used to confirm the structures of the linear aliphatic diamine-based benzoxazine monomers. The spectra in Figure 5 show characteristic resonances of the oxazine ring centered at approximately 3.94 and 4.84 ppm, which are attributed to $\text{O}-\text{CH}_2-\text{N}$ and $\text{Ar}-\text{CH}_2-\text{N}$, respectively.⁸ The original substitution of the alkoxy group in the phenol affects the symmetry of the molecule, resulting in three possible regioisomers: 5,5'; 7,7'; 5,7'. The presence of a mixture of isomers in the product is confirmed by the resonances in the aromatic region. Integration and J coupling analysis show that substitution at the 7-position is favored over substitution at the 5-position in a 3:1 ratio. It should be mentioned that NMR analysis does not allow one to distinguish the 5,7' isomer from those of 5,5' or 7,7' as the resonances in 5,7' completely

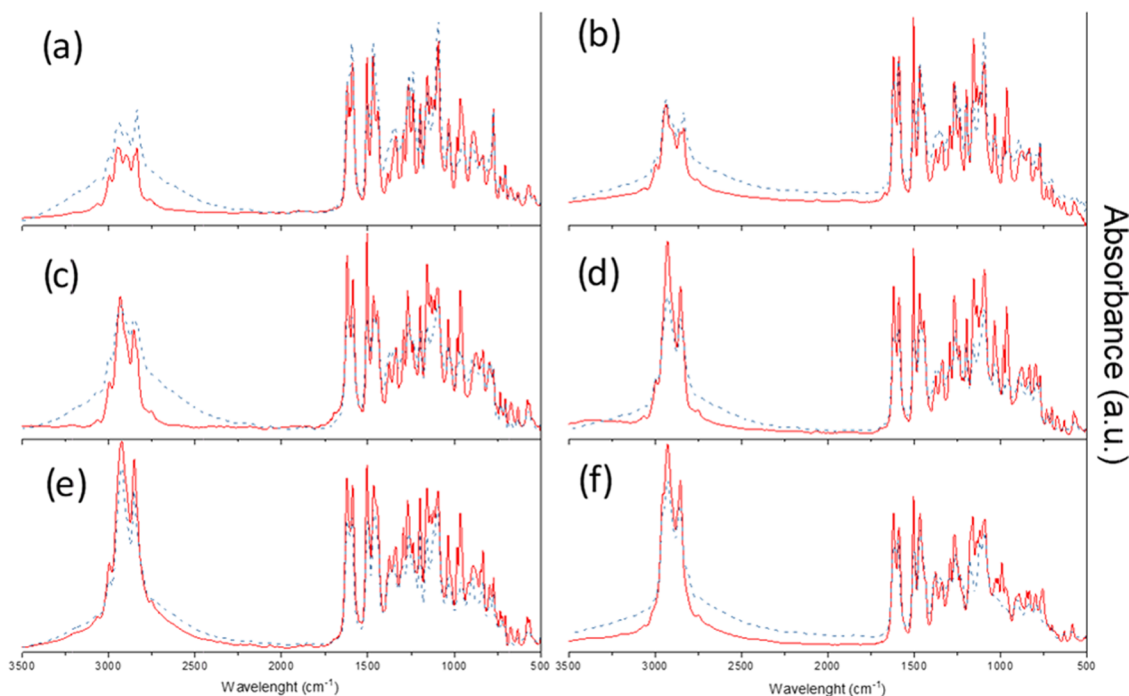


Figure 6. FT-IR spectra of (a) 3MOP-daC2, (b) 3MOP-daC4, (c) 3MOP-daC6, (d) 3MOP-daC8, (e) 3MOP-daC12, (f) 3BOP-daC12 where the solid lines correspond to the monomers and the dashed lines correspond to the material polymerized for 2 h at 120 °C.

overlap with those of 5,5' or 7,7' positions. This favorable 7-position placement is likely due to the $-OR$ group being on the 5-position. With increasing chain length, trends in the NMR spectra are observed. For example, the signals from the alkyl protons become broader and more complex. Furthermore, the double doublet that is observed around 6.3 ppm becomes less symmetric with increasing chain length. The triplet directly downstream of this signal shifts upstream as the alkyl chain length increases such that in 3MOP-daC8 the triplet begins to merge with the double doublet.

3.1.2. Infrared Analysis. The FT-IR spectra for all of the diamine-based benzoxazines show great similarity, except for the expected intensity differences in the aliphatic CH_2 group-related bands. In Figure 6, for all cases, the band around 966 cm^{-1} confirms the presence of the characteristic $N-CH_2-O$ benzoxazine bonds.^{20l} The bands around 1030 and 1156 cm^{-1} represent the presence of the aromatic ether of the benzene ring. These three peaks begin to decrease during polymerization as the oxazine ring opens. The band around 1377 cm^{-1} represents the wagging of the hydrogen atoms in the fourth position, and this band also decreases with polymerization because of the opening of the oxazine ring. The bands around 1500 and 1620 cm^{-1} are characteristic modes of a trisubstituted benzene ring. These bands decrease during polymerization as the ring becomes tetrasubstituted, confirming successful polymerization. The broad bands between 2730 and 3030 cm^{-1} are consistent with the $C-H$ stretches in the alkyl chain, the methoxy or butoxy substituent, and the aromatic benzoxazine ring.^{14a-d}

3.1.3. Shelf-Life. A total of approximately 2.5 kg of 3BOP-daC12 monomer was prepared in eight batches during the project and stored in a freezer until needed for sample fabrication. For composite fabrication, the monomer was removed from the freezer and remained at room temperature for 4–6 h during thawing, handling, and preparation of the composite. The monomer was then returned to the freezer.

Some samples were stored for longer than 3 months and experienced as many as 12 freeze/thaw cycles. The length of storage and repeated thawing and refreezing of the resin had no noticeable effects on viscosity, rheology, or processability.

3.1.4. Polymerization Behavior. The effects of the phenol substitution and the diamine chain length on the polymerization behavior were studied using DSC. Thermograms are shown below in Figure 7. The DSC polymerization exotherms for the diamine-based series of benzoxazine monomers reveal that these compounds have several overlapping peaks, indicating separate processes are contributing to the overall polymerization exotherm. Also, given that each sample is a mixture of isomers widening of the exothermic peak was expected. This can be seen in the thermogram below and has also been reported in the literature.^{13b} The extremely low exotherm exhibited by 3MOP-daC2 has been previously attributed to the short ethane chain, which increases the steric hindrance of the molecule: destabilizing the oxazine rings and lowering the polymerization temperature.^{20m,21}

To help support the experimental results, 5-butoxy-3-butyl-3,4-dihydro-2H-benzo[*e*][1,3]oxazine (abbreviated as PH-bb) and 3-butyl-3,4-dihydro-2H-benzo[*e*][1,3]oxazine (abbreviated as PH-b) were chosen as model compounds using a Gaussian simulation to determine the collective natural charge of the phenol ring and the oxygen in the oxazine ring of the compound. Although the benzoxazine actually used for composite manufacturing was a bisoxazine, a mono-oxazine system, PH-bb, was chosen as the model system to simplify the calculation. The molecular structures for PH-b and PH-bb are shown in Figure 8. This simulation showed that PH-bb's natural charge (-0.0929 eV) is 0.0396 less than the natural charge of PH-b (-0.0907 eV), so that the difference in natural charge between the two compounds is 0.0022 eV .

A similar study was done on 3-phenyl-3,4-dihydro-2H-benzo[*e*][1,3]oxazine (abbreviated as PH-a) where different para substituted PH-a molecules were simulated using the

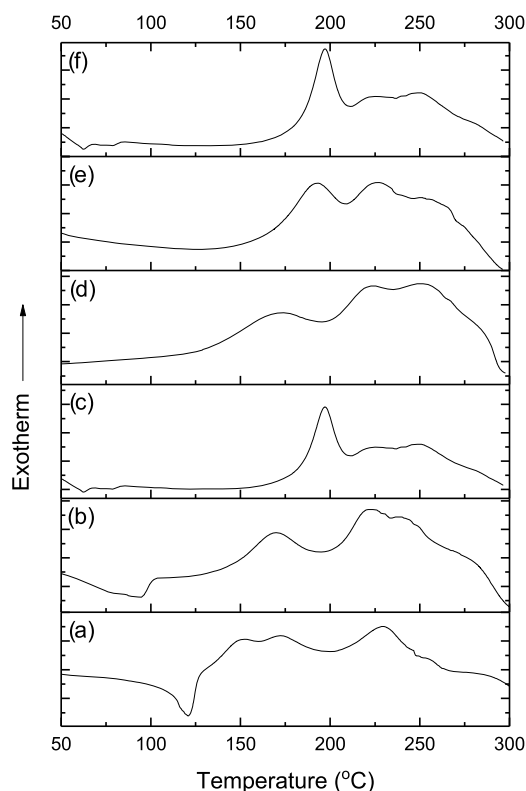


Figure 7. DSC thermograms of (a) 3MOP-daC2, (b) 3MOP-daC4, (c) 3MOP-daC6, (d) 3MOP-daC8, (e) 3MOP-daC12, and (f) 3BOP-daC12.

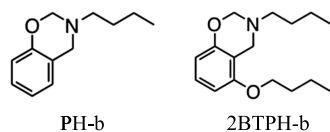


Figure 8. Molecular structure of benzoxazine resins used for Gaussian simulation.

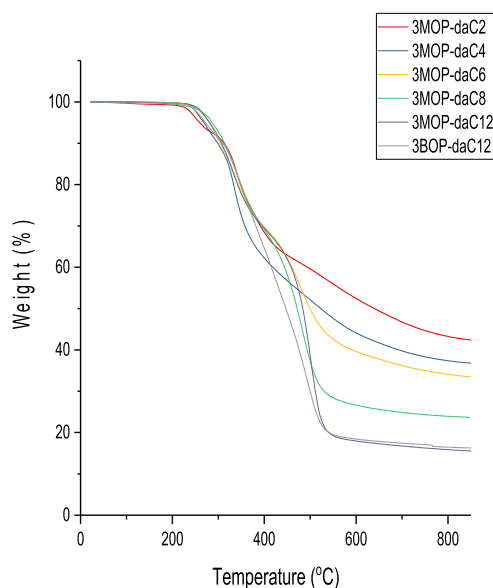


Figure 9. TGA thermograms of polybenzoxazines derived from (a) 3MOP-daC2, (b) 3MOP-daC4, (c) 3MOP-daC6, (d) 3MOP-daC8, (e) 3MOP-daC12, and (f) 3BOP-daC12.

Gaussian program.²² The relationship between the two compounds is nonlinear so an exact comparison between PH-b and PH-a is difficult; however, qualitative results can be obtained.

Using PH-a as reference, the largest difference in natural charge is 0.0088 eV, which results from a meta-substituted nitro group on the phenol ring. This nitro-substituted group has a polymerization temperature of 209 °C, which is 61 °C less than the polymerization temperature of PH-a. The difference in natural charge between PH-b and 2BTTPH-b (−0.0022 eV) is a quarter of the largest difference obtained for PH-a (0.0088 eV). As mentioned before, it is difficult to predict the exact difference in polymerization temperature from the PH-a study, but because the natural charge decreases from PH-b and 2BTTPH-b, a decrease in polymerization temperature from PH-b to 2BTTPH-b is expected.

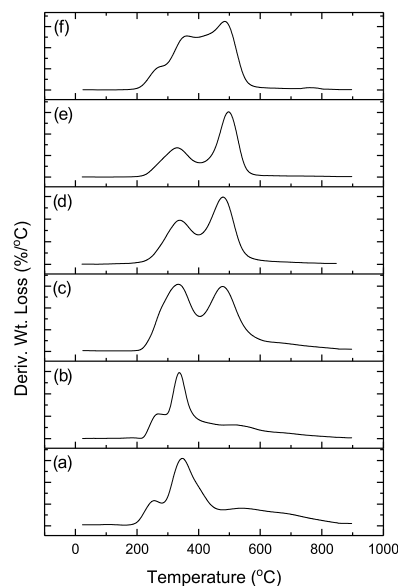
3.2. Properties of Polybenzoxazines and UHMWPE Fiber-Reinforced Polybenzoxazines.

3.2.1. Thermal Stability. TGA was used to study the thermal stability of polymers derived from the meta-substituted benzoxazines. Samples were polymerized for 2 h at 120 °C. TGA thermograms and derivative weight loss thermograms are shown in Figure 9. Degradation temperature and char yield results are summarized in Table 2. Literature values for

Table 2. Degradation Temperatures and Char Yields for Polybenzoxazines and UHMWPE

	T_{ds} (°C)	T_{d10} (°C)	char yield (%)
poly(3MOP-daC2)	260	313	43.3
poly(3MOP-daC4)	269	299	37.4
poly(3MOP-daC6)	281	304	34.1
poly(3MOP-daC8)	286	314	23.9
poly(3MOP-daC12)	281	307	15.9
poly(3BOP-daC12)	272	310	16.5
UHMWPE	431	466	0.11

UHMWPE are included in Table 2 for reference.²³ Degradation temperature was evaluated by determining the



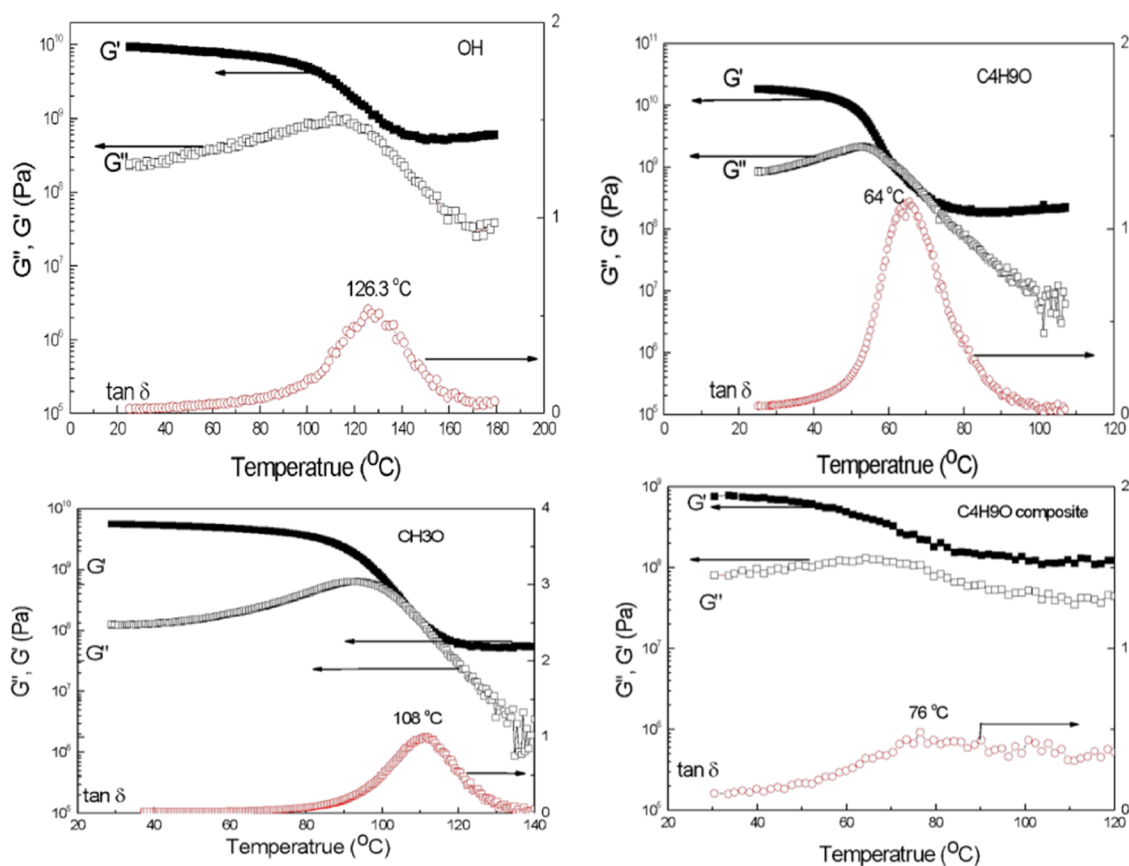


Figure 10. DMA spectra of polybenzoxazines derived from PH-daC12, 3BOP-daC12, 3MOP-daC12, and the UHMWPE fiber/poly(3BOP-daC12) composite.

temperature at which 5% weight loss (T_{d5}) and 10% weight loss (T_{d10}) occurred. The char yield was also determined for each sample. Char yield is defined as the percent residual weight at 800 °C under nitrogen atmosphere. A trend of decreasing char yield for samples with longer alkyl chains was observed. This trend was attributed to the fact that benzoxazines with longer alkyl chains have lower concentrations of aromatics in the molecule. However, the high molecular weight and presence of rigid aromatic structures appear to be sufficient to enhance the thermal stability to an extent greater than that of UHMWPE. A comparison between poly(3MOP-daC12) and poly(3BOP-daC12) shows a small improvement in the thermal stability of the latter.

From the derivative weight loss curves as well as the T_{d5} temperature, it is apparent that diamine chain length has some influence on the onset temperature of thermal degradation. From the data presented, it appears that with the exception of poly(3MOP-daC12) and poly(3BOP-daC12), thermal stability slightly increases with increased diamine chain length, whereas the char yield significantly decreases. In the case of poly(3BOP-daC12), the onset of degradation is even lower due to the presence of the longer butyl chain compared to the methyl group. Despite a significant decrease in char yield compared to typical polybenzoxazines, the observed char yields are remarkably higher than usual aliphatic compounds, which typically exhibit near-zero char yields.

3.2.2. Dynamic Mechanical Properties. Dynamic mechanical analysis (DMA) was performed to study the change in viscoelastic properties resulting from substitutions of the phenol. Three polybenzoxazine samples, poly(PH-daC12),

poly(3MOP-daC12), and poly(3BOP-daC12), were prepared from 1,12-diaminododecane and three different phenols (an unsubstituted phenol, a *meta*-methoxyphenol, and a *meta*-butoxyphenol). A composite was also formed using poly(3BOP-daC12) and UHMWPE fabric. The results from this experiment are shown in Figure 10, and the glass transition temperatures (T_g) observed for each polybenzoxazine are listed in Table 3.

The broad $\tan \delta$ peaks that were observed suggest that the polymers experience glass transitions over a wide temperature

Table 3. Glass Transition Temperatures from DMA

	T_g (°C)
poly(PH-daC12)	126
poly(3BOP-daC12)	64
poly(3MOP-daC12)	106
poly(3BOP-daC12) composite	76

range. This may be attributed to slight structural variations caused by the isomer mixture. Poly(3MOP-daC12) exhibited a longer glassy region and a shorter rubbery region than poly(3BOP-daC12). In both the *meta*-methoxy- and *meta*-butoxy-substituted compounds, the loss and storage moduli overlap in the transition region.

3.2.3. ^1H NMR Study of Polymer Structure. Nuclear magnetic resonance spectroscopy (^1H NMR) was used to further investigate the polymerization mechanism of this family of benzoxazines. For this study, 3MOP-daC2, 3MOP-daC4, 3MOP-daC6, and 3MOP-daC8 were polymerized for 2 h at

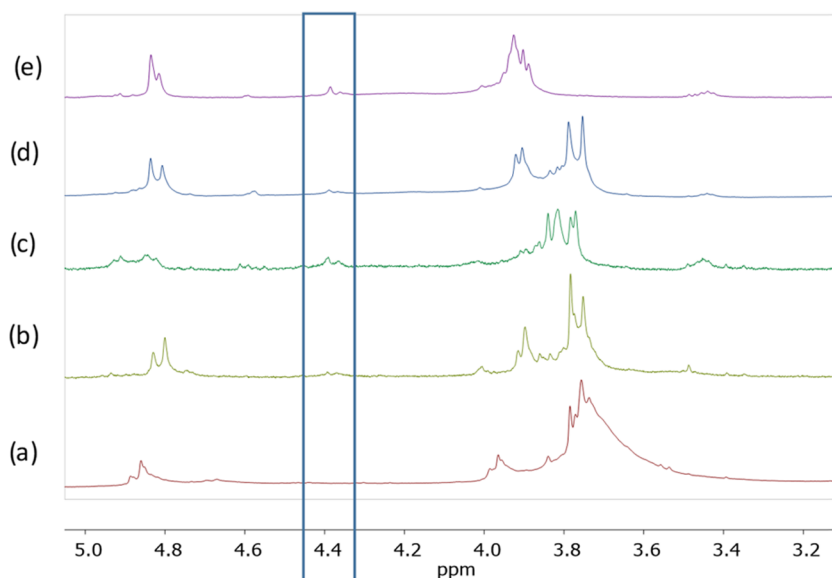


Figure 11. ^1H NMR spectra in CDCl_3 of (a) poly(3MOP-daC2), (b) poly(3MOP-daC6), and (c) poly(3MOP-daC8) cured at $120\text{ }^\circ\text{C}$ for 2 h and (d) poly(3MOP-daC12), (e) poly(3BOP-daC12) cured at $120\text{ }^\circ\text{C}$ for 1 h.

$120\text{ }^\circ\text{C}$, whereas 3MOP-daC12 and 3BOP-daC12 were polymerized for 1 h at $120\text{ }^\circ\text{C}$, making it possible to dissolve the samples in CDCl_3 . In a previous study reported by Liu et al.,^{14c} it was proposed that the presence of a peak around 4.3 ppm is indicative of phenolic CH_2 units originating from a nitrogen attaching to the ortho position on the phenol. In Figure 11, it is clear that the characteristic benzoxazine resonances at 3.90–3.97 and 4.80–4.87 ppm are still present, which implies that not all oxazine rings have undergone the ring-opening reaction. For all cases, except 3MOP-daC2, it is also possible to observe a resonance around 4.34 ppm, which is consistent with the proposed phenolic structure for the PBZ. This result is consistent with the DSC observations, which suggest a different mechanistic pathway for 3MOP-daC2 compared to all of the other benzoxazines in this family that we studied. Poly(3MOP-daC4) did not sufficiently dissolve in CDCl_3 to obtain a clear spectrum. Figure 12 shows molecular models with other possible methylene generated by different mechanistic pathways.

3.3. Estimation of Hydrogen Concentration. Polybenzoxazines developed during this project were tailored at the

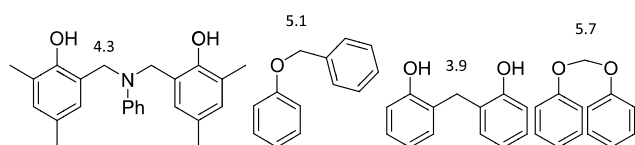


Figure 12. Chemical shift of methylene groups in ppm for model compounds previously reported.^{2,24}

molecular level to possess high concentrations of hydrogen per unit volume. A simple formula, based on the number of hydrogen atoms in the repeat unit, the polymer density, and the molecular weight, was used to estimate hydrogen concentration in each polybenzoxazine formulation. To obtain density values, polybenzoxazine samples were polymerized for 2 h at $120\text{ }^\circ\text{C}$ and then weighed in air and while submerged in water, providing the density by way of Archimedes' Principle.

The following formula was then used to calculate the hydrogen concentration in each compound

$$\text{H concentration} = N_{\text{H}} \times N_{\text{Av}} \times \frac{\rho}{\text{MW}_{\text{repeat unit}}}$$

where N_{H} is the number of hydrogen atoms per repeat unit of the polymer, N_{Av} is Avogadro's number (6.022×10^{23} repeat units/mol), ρ is the density of the polymer in g/cm^3 , and $\text{MW}_{\text{repeat unit}}$ is the molar mass of the repeat unit of the polymer in g/mol . The final units for hydrogen concentration are expressed as $(\text{H atoms}/\text{cm}^3) \times 10^{23}$.

The densities obtained from the displacement tests are listed in Table 4 along with other parameters used in the calculation. The calculated hydrogen concentration for each compound is provided in Table 5.

Table 4. Parameters Used To Calculate Estimated Hydrogen Concentration in Polybenzoxazines

	no. of H atoms per repeat unit	density (g/cm^3)	molecular weight of repeat unit (g/mol)
poly(3MOP-daC4)	28	1.03	384.476
poly(3MOP-daC6)	32	1.07	412.530
poly(3MOP-daC8)	36	1.08	440.584
poly(3MOP-daC12)	44	1.12	496.692
poly(3BOP-daC12)	56	1.07	580.854

Table 5. Estimated Hydrogen Concentration in Alkoxy-diamino-polybenzoxazines

	hydrogen concentration ($\text{H atoms}/\text{cm}^3 \times 10^{23}$)
poly(3MOP-daC4)	0.451
poly(3MOP-daC6)	0.501
poly(3MOP-daC8)	0.531
poly(3MOP-daC12)	0.595
poly(3BOP-daC12)	0.622
poly(BNP-diC12)	0.673
poly(BPA-diC12)	0.625

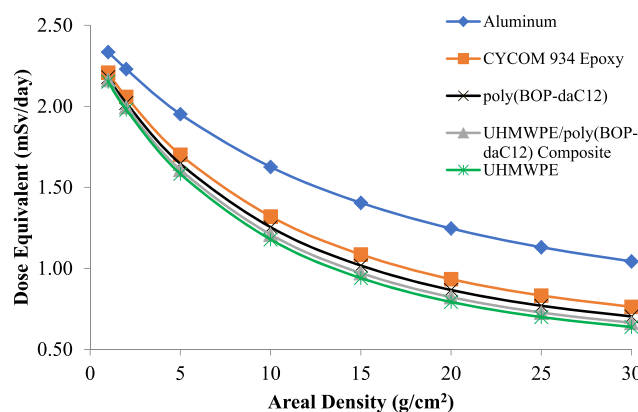
Table 6. List of Materials and Modeling Parameters Used in On-Line Tool for the Assessment of Radiation in Space (OLTARIS) Simulations

material type	molecular formula	density (g/cm ³)
aluminum (OLTARIS default material)	Al	2.70
polyethylene (UHMWPE)	CH ₂	0.97
epoxy (Cytec CYCOM 934)	C ₃₇ H ₄₂ N ₄ O ₆ S	1.30
poly(3BOP-daC12) polybenzoxazine	C ₃₆ H ₅₆ N ₂ O ₄	1.07
UHMWPE fiber/poly(3BOP-daC12) composite	CH ₂ (60 vol %)/C ₃₆ H ₅₆ N ₂ O ₄ (40 vol %)	1.01

These results indicate a trend of increasing density with increasing alkyl chain length for polybenzoxazines based on methoxyphenol, which also impacts increase in hydrogen concentration. For poly(3BOP-daC12), the lower density is compensated by the increase in hydrogen atoms per repeat unit, which results in an increase in hydrogen concentration compared to the methoxyphenol-based polybenzoxazines. Compared to poly(BNP-diC12) and poly(BPA-diC12), polybenzoxazines developed during the initial stage of this project, hydrogen concentrations in the methoxyphenol- and butoxyphenol-based polybenzoxazines are slightly lower. However, it is important to reiterate that the earlier materials were not viable due to incomplete polymerization and short shelf-life.

3.4. Simulated Shielding Performance for Poly(3BOP-daC12). An assessment of the potential radiation shielding performances of poly(3BOP-daC12) and the UHMWPE fiber/poly(3BOP-daC12) composite was performed using NASA's On-Line Tool for the Assessment of Radiation in Space (OLTARIS).²⁵ The two materials were modeled in OLTARIS and subjected to simulated free-space environments containing galactic cosmic rays (GCRs) and solar particle events (SPEs). For GCR free-space simulations, the Badhwar-O'Neill 2010 GCR model and 1977 solar minimum event parameters were selected. For SPE free-space simulations, the August 1972 (King) event parameter was selected. GCR and SPE simulation parameters were selected based on their use as cross-program design specifications for natural environments.²⁶ Benchmark shielding materials were also modeled and used for comparison. The materials and modeling parameters used in OLTARIS simulations are provided in Table 6. The benchmark epoxy material used in simulations was Cytec CYCOM 934 (formerly Fiberite 934), which is referenced by NASA radiation shielding literature²⁷ and is the matrix resin used in the default graphite-epoxy composite found in OLTARIS.

Radiation shielding performance curves were developed by modeling materials using the slab geometry option and performing multiple simulations with slabs of increasing areal density from 1.0 to 30.0 g/cm². Performance curves for the GCR environment are shown below in Figure 13. Shielding performance is determined by examining the equivalent radiation dose (in mSv/day) for all materials at a given areal density. A lower radiation dose indicates better shielding performance. It is evident from these curves that the shielding performance of the hydrogen-rich poly(3BOP-daC12) polybenzoxazine is approaching that of polyethylene. Poly(3BOP-daC12) provides superior radiation shielding properties compared to the benchmark epoxy. The performance curve of the UHMWPE fiber/poly(3BOP-daC12) composite material is shifted even closer to the polyethylene benchmark curve. The level of improvement is provided by the increased hydrogen concentration in the UHMWPE fibers and is directly related to the amount of fiber contained within the composite;

**Figure 13.** OLTARIS-simulated radiation shielding performance results for the GCR free-space environment.

as the volume fraction of fiber increases so too does the shielding performance. A fiber volume fraction of 60% was used for the simulation, which is typical for polymer matrix composites.

3.5. Tensile Properties of UHMWPE Fiber/Poly(3BOP-daC12) Composites. Tensile testing of UHMWPE fiber/poly(3BOP-daC12) composite samples was performed to evaluate tensile strength, tensile modulus, Poisson's ratio, and tensile strain at failure. A total of 18 specimens were tested in accordance with ASTM D3039, using three different environmental conditions (six specimens per condition). Temperature and relative humidity parameters for each environmental condition are listed in Table 7. Test specimens were laser cut

Table 7. Tensile Testing Environmental Conditions

environmental condition	temperature	relative humidity
RTD (room temperature, dry)	23 °C (70 °F)	50%
CTD (cold temperature, dry)	-50 °C (-58 °F)	N/A
ETW (elevated temperature, wet)	80 °C (176 °F)	85%

from two 254 mm × 254 mm × 1.5 mm composite plates that were each comprised of eight plies of plain-woven Spectra 1000 UHMWPE fabric (Style 932). Nominal test specimen dimensions were 254 mm × 25.4 mm × 1.5 mm. A summary of the mechanical properties obtained from this testing is provided in Table 8. The results show excellent tensile properties suitable for structural or semistructural applications.

4. CONCLUSIONS

A systematic study of diamine-based benzoxazines synthesized from phenols substituted in the meta position by alkoxy groups shows the creation of polymers with relatively low polymerization temperature for processing and adequate shelf-life (when stored under refrigerated conditions).

Table 8. UHMWPE Fiber/poly(3BOP-daC12) Composite Tensile Properties (Average Values Reported)

property	composite layup	environmental condition		
		CTD	RTD	ETW
tensile strength, 0° (MPa)	[0] ₈	615	493	239
tensile modulus (chord, 0.1–0.3% strain), 0° (MPa)	[0] ₈	13 306	875	2806
tensile strain at failure, 0° (%)	[0] ₈		6.90	
Poisson's ratio	[0] ₈	0.100	0.118	0.116

The DSC and TGA studies demonstrate the influence of the diamine chain length on the reactivity of the benzoxazines and the stability of the thermoset. The observed trend indicates that a longer chain will increase the polymerization temperature, whereas simultaneously decreasing the thermal stability of the polymer. The hydrogen concentration for 3BOP-daC12 proves to be high enough to provide adequate shielding capabilities compared to polyethylene and superior shielding properties to epoxy (Cytac CYCOM 934). The composite material UHMWPE fiber/poly(3BOP-dac12) further improves this behavior making it comparable to UHMWPE, which was the main goal of this project. As a multifunctional material, the UHMWPE fiber/poly(3BOP-daC12) composite offers a unique and attractive combination of high-strength and excellent radiation shielding performance. NASA plans to send samples of UHMWPE fiber/poly(3BOP-dac12) composites to the International Space Station as part of Materials International Space Station Experiment 12 (MISSE-12). MISSE-12 is scheduled to begin in the fall of 2019 and continue for a duration of 1 year. Empirical data related to radiation shielding performance are anticipated from this testing.

AUTHOR INFORMATION

Corresponding Author

*E-mail: hxi3@cwru.edu.

ORCID

Scott Winroth: 0000-0002-2648-9858

Hatsuo Ishida: 0000-0002-2590-2700

Author Contributions

The manuscript was written based on contributions of all authors. All authors have given approval to the submitted version of the manuscript.

Notes

The authors declare no competing financial interest.

All of the works on pure resins for both benzoxazine monomers and polymers, such as synthesis, molecular and thermal characterization, were performed at the Department of Macromolecular Science in Case Western University, Cleveland, Ohio. All of the works related to UHMWPE fiber-reinforced polybenzoxazines, such as processing and mechanical property determination were done at Material Answers LLC in Weston, Massachusetts. Additionally, they also performed galactic cosmic ray simulation.

ACKNOWLEDGMENTS

The authors gratefully acknowledge the financial support by NASA under award No(s) NNX14CL25P and NNX15CL03C.

REFERENCES

(1) Hong, H. Y.; Ishida, H. Mechanistic study on the thermal decomposition of polybenzoxazines Effects of aliphatic amines. *J. Polym. Sci., Part B: Polym. Phys.* **1998**, *36*, 1935–1946.

(2) Ishida, H.; Allen, D. J. Physical and mechanical characterization of near-zero shrinkage polybenzoxazines. *J. Polym. Sci., Part B: Polym. Phys.* **1996**, *34*, 1019–1030.

(3) (a) Kiskan, B.; Yagci, Y.; Ishida, H. Synthesis, characterization, and properties of new thermally curable polyetheresters containing benzoxazine moieties in the main chain. *J. Polym. Sci., Part A: Polym. Chem.* **2008**, *46*, 414–420. (b) Kumar, K. S. S.; Nair, C. P. R.; Sadhana, R.; Ninan, K. N. Benzoxazine–bismaleimide blends: Curing and thermal properties. *Eur. Polym. J.* **2007**, *43*, 5084–5096. (c) Zhang, K.; Han, L.; Nie, Y.; Szigeti, M. L.; Ishida, H. Examining the effect of hydroxyl groups on the thermal properties of polybenzoxazines: using molecular design and Monte Carlo simulation. *RSC Adv.* **2018**, *8*, 18038–18050. (d) Dueramae, I.; Jubsilp, C.; Takeichi, T.; Rimdusit, S. High thermal and mechanical properties enhancement obtained in highly filled polybenzoxazine nanocomposites with fumed silica. *Composites, Part B* **2014**, *56*, 197–206.

(4) (a) Ning, X.; Ishida, H. Phenolic materials via ring-opening polymerization of benzoxazines: Effect of molecular structure on mechanical and dynamic mechanical properties. *J. Polym. Sci., Part B: Polym. Phys.* **1994**, *32*, 921–927. (b) Allen, D. J.; Ishida, H. Physical and mechanical properties of flexible polybenzoxazine resins: Effect of aliphatic diamine chain length. *J. Appl. Polym. Sci.* **2006**, *101*, 2798–2809. (c) Ishida, H.; Allen, D. J. Mechanical characterization of copolymers based on benzoxazine and epoxy. *Polymer* **1996**, *37*, 4487–4495. (d) Krishnan, S.; Arumugam, H.; Kuppan, C.; Goswami, A.; Chavali, M.; Muthukaruppan, A. Silane-functionalized polybenzoxazines: A superior corrosion resistant coating for steel plates. *Mater. Corros.* **2017**, *68*, 1343–1354.

(5) (a) Ishida, H.; Agag, T. *Handbook of Benzoxazine Resins*; Elsevier, 2011. (b) Ghosh, N. N.; Kiskan, B.; Yagci, Y. Polybenzoxazines—New high performance thermosetting resins: Synthesis and properties. *Prog. Polym. Sci.* **2007**, *32*, 1344–1391. (c) Endo, T.; Sudo, A. Molecular Designs of Benzoxazines With Enhanced Reactivity Based on Utilization of Neighboring-Group Participation and Introduction of Thioether Moiety. In *Advanced and Emerging Polybenzoxazine Science and Technology*; Ishida, H., Froimowicz, P., Eds.; Elsevier: Amsterdam, 2017; Chapter 3, pp 23–33.

(6) (a) Borggräfe, A.; Quatmann, M.; Nölke, D. Radiation protective structures on the base of a case study for a manned Mars mission. *Acta Astronaut.* **2009**, *65*, 1292–1305. (b) Thibeault, S. A.; Kang, J. H.; Sauti, G.; Park, C.; Fay, C. C.; King, G. C. Nanomaterials for radiation shielding. *MRS Bull.* **2015**, *40*, 836–841. (c) Li, X.; Warden, D.; Bayazitoglu, Y. Analysis to Evaluate Multilayer Shielding of Galactic Cosmic Rays. *J. Thermophys. Heat Transfer* **2018**, *32*, 525–531.

(7) Churhill, R. J.; Aquino, E. C.; OrWoll, R.; Kiefer, R.; Groger, H. P. Nanostructured Additives to High-Performance Polymers for Use in Radiation Shielding, Protection against Atomic Oxygen and in Structural Applications. US0161564A12013.

(8) (a) Nambiar, S.; Yeow, J. T. W. Polymer-Composite Materials for Radiation Protection. *ACS Appl. Mater. Interfaces* **2012**, *4*, 5717–5726. (b) Kaul, R. K.; Barghouty, A. F.; Dahche, H. M. Space Radiation Transport Properties of Polyethylene-Based Composites. *Ann. N. Y. Acad. Sci.* **2004**, *1027*, 138–149. (c) Singleterry, R. C.; Thibeault, S. A. *Materials for Low-Energy Neutron Radiation Shielding*, TP-2000-210281; NASA, 2000.

- (9) Kaul, R. K.; Barghouty, A. F.; Penn, B. G.; Hulcher, A. B. Multi-functional Layered Structure Having Structural and Radiation Shielding Attributes. US7,855,157B1, 2008.
- (10) Guetersloh, S.; Zeitlin, C.; Heilbronn, L.; Miller, J.; Komiyama, T.; Fukumura, A.; Iwata, Y.; Murakami, T.; Bhattacharya, M. Polyethylene as a radiation shielding standard in simulated cosmic-ray environments. *Nucl. Instrum. Methods Phys. Res., Sect. B* **2006**, *252*, 319–332.
- (11) Cucinotta, F. A.; Wilson, J. W.; Williams, J. R.; Dicello, J. F. Analysis of MIR-18 results for physical and biological dosimetry: radiation shielding effectiveness in LEO. *Radiat. Meas.* **2000**, *32*, 181–191.
- (12) (a) Shavers, M. R.; Zapp, N.; Barber, R. E.; Wilson, J. W.; Qualls, G.; Toupe, L.; Ramsey, S.; Vinci, V.; Smith, G.; Cucinotta, F. A. Implementation of ALARA radiation protection on the ISS through polyethylene shielding augmentation of the Service Module Crew Quarters. *Adv. Space Res.* **2004**, *34*, 1333–1337. (b) Miller, J.; Zeitlin, C.; Cucinotta, F. A.; Heilbronn, L.; Stephens, D.; Wilson, J. W. Benchmark studies of the effectiveness of structural and internal materials as radiation shielding for the international space station. *Radiat. Res.* **2003**, *159*, 381–390.
- (13) (a) Froimowicz, P.; Zhang, K.; Ishida, H. Intramolecular Hydrogen Bonding in Benzoxazines: When Structural Design Becomes Functional. *Chem. – Eur. J.* **2016**, *22*, 2691–2707. (b) Liu, J.; Ishida, H. Anomalous Isomeric Effect on the Properties of Bisphenol F-based Benzoxazines: Toward the Molecular Design for Higher Performance. *Macromolecules* **2014**, *47*, 5682–5690.
- (14) (a) Dunkers, J.; Ishida, H. Reaction of benzoxazine-based phenolic resins with strong and weak carboxylic acids and phenols as catalysts. *J. Polym. Sci., Part A: Polym. Chem.* **2000**, *37*, 1913–1921. (b) Wang, Y. X.; Ishida, H. Cationic ring-opening polymerization of benzoxazines. *Polymer* **1999**, *40*, 4563–4570. (c) Sudo, A.; Kudoh, R.; Nakayama, H.; Arima, K.; Endo, T. Selective Formation of Poly(N,O-acetal) by Polymerization of 1,3-Benzoxazine and Its Main Chain Rearrangement. *Macromolecules* **2008**, *41*, 9030–9034. (d) Chutayothin, P.; Ishida, H. Cationic Ring-Opening Polymerization of 1,3-Benzoxazines: Mechanistic Study Using Model Compounds. *Macromolecules* **2010**, *43*, 4562–4572. (e) Liu, C.; Shen, D.; Sebastián, R. M.; Marquet, J.; Schönfeld, R. Mechanistic Studies on Ring-Opening Polymerization of Benzoxazines: A Mechanistically Based Catalyst Design. *Macromolecules* **2011**, *44*, 4616–4622. (f) Han, L.; Salum, M. L.; Zhang, K.; Froimowicz, P.; Ishida, H. Intrinsic self-initiating thermal ring-opening polymerization of 1,3-benzoxazines without the influence of impurities using very high purity crystals. *J. Polym. Sci., Part A: Polym. Chem.* **2017**, *55*, 3434–3445. (g) Özalp, T. F.; Catak, S.; Kiskan, B.; Yagci, Y.; Aviyente, V. Rationalizing the regioselectivity of cationic ring-opening polymerization of benzoxazines. *Eur. Polym. J.* **2018**, *105*, 61–67. (h) Wang, H.; Zhu, R.; Yang, P.; Gu, Y. A study on the chain propagation of benzoxazine. *Polym. Chem.* **2016**, *7*, 860–866.
- (15) Velez-Herrera, P.; Ishida, H. Low temperature polymerization of novel, monotropic liquid crystalline benzoxazines. *J. Polym. Sci., Part A: Polym. Chem.* **2009**, *47*, 5871–5881.
- (16) Chernykh, A.; Agag, T.; Ishida, H. Effect of Polymerizing Diacetylene Groups on the Lowering of Polymerization Temperature of Benzoxazine Groups in the Highly Thermally Stable, Main-Chain-Type Polybenzoxazines. *Macromolecules* **2009**, *42*, 5121–5127.
- (17) (a) Kudoh, R.; Sudo, A.; Endo, T. A Highly Reactive Benzoxazine Monomer, 1-(2-Hydroxyethyl)-1,3-Benzoxazine: Activation of Benzoxazine by Neighboring Group Participation of Hydroxyl Group. *Macromolecules* **2010**, *43*, 1185–1187. (b) Zhang, K.; Han, L.; Froimowicz, P.; Ishida, H. A Smart Latent Catalyst Containing o-Trifluoroacetamide Functional Benzoxazine: Precursor for Low Temperature Formation of Very High Performance Polybenzoxazole with Low Dielectric Constant and High Thermal Stability. *Macromolecules* **2017**, *50*, 6552–6560. (c) Zhang, K.; Froimowicz, P.; Han, L.; Ishida, H. Hydrogen-bonding characteristics and unique ring-opening polymerization behavior of Ortho-methylol functional benzoxazine. *J. Polym. Sci., Part A: Polym. Chem.* **2016**, *54*, 3635–3642. (d) Liu, Y.; Hao, Z.; Lv, S.; Huang, J.; Liao, C.; Run, M. Structural effects of diamines on synthesis, polymerization, and properties of benzoxazines based on o-allylphenol. *Polymer* **2015**, *57*, 29–38.
- (18) (a) Agag, T.; Liu, J.; Graf, R.; Spiess, H. W.; Ishida, H. Benzoxazole Resin: A Novel Class of Thermoset Polymer via Smart Benzoxazine Resin. *Macromolecules* **2012**, *45*, 8991–8997. (b) Zhang, K.; Liu, J.; Ishida, H. An Ultrahigh Performance Cross-Linked Polybenzoxazole via Thermal Conversion from Poly(benzoxazine amic acid) Based on Smart o-Benzoxazine Chemistry. *Macromolecules* **2014**, *47*, 8674–8681. (c) Zhang, K.; Ishida, H. Smart synthesis of high performance thermosets based on ortho-(amide-co-imide) functional benzoxazines. *Front. Mater.* **2015**, *2*, 1–9. (d) Zhang, K.; Ishida, H. An anomalous trade-off effect on the properties of smart ortho-functional benzoxazines. *Polym. Chem.* **2015**, *6*, 2541–2550. (e) Lin, R.; Zhu, Y.; Zhang, Y.; Wang, L.; Yu, S. Pyrogallol-based benzoxazines with latent catalytic characteristics: The temperature-dependent effect of hydrogen bonds on ring-opening polymerization. *Eur. Polym. J.* **2018**, *102*, 141–150.
- (19) (a) Sudo, A.; Hirayama, S.; Endo, T. Highly efficient catalysts-acetylacetonato complexes of transition metals in the 4th period for ring-opening polymerization of 1,3-benzoxazine. *J. Polym. Sci., Part A: Polym. Chem.* **2010**, *48*, 479–484. (b) Sudo, A.; Mori, A.; Endo, T. Promoting effects of urethane derivatives of phenols on the ring-opening polymerization of 1,3-benzoxazines. *J. Polym. Sci., Part A: Polym. Chem.* **2011**, *49*, 2183–2190. (c) Sudo, A.; Yamashita, H.; Endo, T. Ring-opening polymerization of 1,3-benzoxazines by p-toluenesulfonates as thermally latent initiators. *J. Polym. Sci., Part A: Polym. Chem.* **2011**, *49*, 3631–3636. (d) Oie, H.; Mori, A.; Sudo, A.; Endo, T. Polyaddition of bifunctional 1,3-benzoxazine and 2-methylresorcinol. *J. Polym. Sci., Part A: Polym. Chem.* **2013**, *51*, 3867–3872. (e) William Kawaguchi, A.; Sudo, A.; Endo, T. Promoting effect of thiophenols on the ring-opening polymerization of 1,3-benzoxazine. *J. Polym. Sci., Part A: Polym. Chem.* **2014**, *52*, 2523–2527. (f) Andreu, R.; Reina, J. A.; Ronda, J. C. Carboxylic acid-containing benzoxazines as efficient catalysts in the thermal polymerization of benzoxazines. *J. Polym. Sci., Part A: Polym. Chem.* **2008**, *46*, 6091–6101. (g) Wang, Y.; Ishida, H. *Methyl p-toluenesulfonate-Initiated Cationic Polymerization of a Benzoxazine Resin*; American Chemical Society, Division of Polymeric Materials: Science and Engineering, 1999. (h) Kocaarslan, A.; Kiskan, B.; Yagci, Y. Ammonium salt catalyzed ring-opening polymerization of 1,3-benzoxazines. *Polymer* **2017**, *122*, 340–346. (i) Arslan, M.; Kiskan, B.; Yagci, Y. Ring-Opening Polymerization of 1,3-Benzoxazines via Borane Catalyst. *Polymers* **2018**, *10*, 239. (j) Arza, C. R.; Froimowicz, P.; Ishida, H. Triggering effect caused by elemental sulfur as a mean to reduce the polymerization temperature of benzoxazine monomers. *RSC Adv.* **2016**, *6*, 35144–35151.
- (20) (a) Ishida, H.; Sanders, D. P. Regioselectivity and Network Structure of Difunctional Alkyl-Substituted Aromatic Amine-Based Polybenzoxazines. *Macromolecules* **2000**, *33*, 8149–8157. (b) Ishida, H.; Sanders Daniel, P. Improved thermal and mechanical properties of polybenzoxazines based on alkyl-substituted aromatic amines. *J. Polym. Sci., Part B: Polym. Phys.* **2000**, *38*, 3289–3301. (c) Wang, X.; Chen, F.; Gu, Y. Influence of electronic effects from bridging groups on synthetic reaction and thermally activated polymerization of bisphenol-based benzoxazines. *J. Polym. Sci., Part A: Polym. Chem.* **2011**, *49*, 1443–1452. (d) Andreu, R.; Reina, J. A.; Ronda, J. C. Studies on the thermal polymerization of substituted benzoxazine monomers: Electronic effects. *J. Polym. Sci., Part A: Polym. Chem.* **2008**, *46*, 3353–3366. (e) Zhu, Y.; Li, M.; Gu, Y. Influence of La₂O₃ on the Thermal Stability of Polybenzoxazine: Effect of Substituted Groups. *J. Macromol. Sci., Part B: Phys.* **2013**, *52*, 738–750. (f) Deng, Y.; Zhang, Q.; Zhou, Q.; Zhang, C.; Zhu, R.; Gu, Y. Influence of substituent on equilibrium of benzoxazine synthesis from Mannich base and formaldehyde. *Phys. Chem. Chem. Phys.* **2014**, *16*, 18341–18348. (g) Wang, M. W.; Jeng, R. J.; Lin, C. H. Study on the Ring-Opening Polymerization of Benzoxazine through Multisubstituted Polybenzoxazine Precursors. *Macromolecules* **2015**, *48*, 530–535.

(h) Nour-Eddine, E. M.; Yuan, Q.; Huang, F. Investigation of curing and thermal behavior of benzoxazine and lignin mixtures. *J. Appl. Polym. Sci.* **2012**, *125*, 1773–1781. (i) Liu, Y.-L.; Chou, C.-I. High performance benzoxazine monomers and polymers containing furan groups. *J. Polym. Sci., Part A: Polym. Chem.* **2005**, *43*, 5267–5282. (j) Das, D. L. J.; Rajeev, R.; Rajeev, R. S.; Kumar, K. S. S. Synthesis, characterization, curing and thermal decomposition kinetics of bisphenol-A based polybenzoxazine. *Int. J. Sci. Technol. Res.* **2013**, *2*, 146–155. (k) Lochab, B.; Varma, I. K.; Bijwe, J. Cardanol-based bisbenzoxazines. *J. Therm. Anal. Calorim.* **2012**, *107*, 661–668. (l) Han, L.; Iguchi, D.; Gil, P.; Heyl, T. R.; Sedwick, V. M.; Arza, C. R.; Ohashi, S.; Lacks, D. J.; Ishida, H. Oxazine Ring-Related Vibrational Modes of Benzoxazine Monomers Using Fully Aromatically Substituted, Deuterated, ¹⁵N Isotope Exchanged, and Oxazine-Ring-Substituted Compounds and Theoretical Calculations. *J. Phys. Chem. A* **2017**, *121*, 6269–6282. (m) Allen, D. J.; Ishida, H. Polymerization of linear aliphatic diamine-based benzoxazine resins under inert and oxidative environments. *Polymer* **2007**, *48*, 6763–6772. (n) Han, L.; Zhang, K.; Ishida, H.; Froimowicz, P. Study of the Effects of Intramolecular and Intermolecular Hydrogen-Bonding Systems on the Polymerization of Amide-Containing Benzoxazines. *Macromol. Chem. Phys.* **2017**, *218*, No. 1600562.

(21) Allen, D. J.; Ishida, H. Effect of phenol substitution on the network structure and properties of linear aliphatic diamine-based benzoxazines. *Polymer* **2009**, *50*, 613–626.

(22) Ohashi, S.; Iguchi, D.; Heyl, T. R.; Gil, P.; Lacks, D. J.; Froimowicz, P.; Ishida, H. Quantitative Studies on the p-Substituent Effect of Phenolic Component on the Polymerization of Benzoxazines. *Polym. Chem.* **2018**, *9*, 4194–4204.

(23) Figueiredo, L. R. F.; Da Silva, L. D.; dos Passos, T. A.; de Lima, S. J. G. In *Effect of Addition of a Quasicrystal Filler on Thermal and Dynamic Mechanical Behavior of Commercial Ultra-High Molecular Weight Polyethylene*, 22nd International Congress of Mechanical Engineering (COBEM 2013), Ribeirão Preto, SP, Brazil, 2013.

(24) (a) Niu, J.; Zhou, H.; Li, Z.; Xu, J.; Hu, S. An Efficient Ullmann-Type C–O Bond Formation Catalyzed by an Air-Stable Copper(I)–Bipyridyl Complex. *J. Org. Chem.* **2008**, *73*, 7814–7817. (b) Ballmann, J.; Fuchs, M. G. G.; Dechert, S.; John, M.; Meyer, F. Synthesis and Coordination Properties of Chelating Dithiophenolate Ligands. *Inorg. Chem.* **2009**, *48*, 90–99. (c) More, S. V.; Ardhapure, S. S.; Naik, N. H.; Bhusare, S. R.; Jadhav, W. N.; Pawar, R. P. Room-Temperature Ionic Liquid-Promoted Williamson's Synthesis of Ethers: A Facile Synthesis of Diaryloxymethanes. *Synth. Commun.* **2005**, *35*, 3113–3118.

(25) Singletery, R. C.; Blattig, S. R.; Cloudsley, M. S.; Qualls, G. D.; Sandridge, C. A.; Simonsen, L. C.; Slaba, T. C.; Walker, S. A.; Badavi, F. F.; Spangler, J. L.; Aumann, A. R.; Neal Zapp, E.; Rutledge, R. D.; Lee, K. T.; Norman, R. B.; Norbury, J. W. OLTARIS: On-line tool for the assessment of radiation in space. *Acta Astronaut.* **2011**, *68*, 1086–1097.

(26) Roberts, B. C. *Cross-Program Design Specification for Natural Environments (DSNE), Space Launch System (SLS) Program*, revision: D, Document No. SLS-SPEC-159; NTRS, 2015.

(27) Wilson, J. W.; Miller, J.; Konradi, A.; Cucinotta, F. A. In *Shielding Strategies for Human Space Exploration*, Proceedings of a Workshop Sponsored by the National Aeronautics and Space Administration, Lyndon B. Johnson Space Center, Houston, Texas, Dec 6–8, 1995; NASA, 1997.